Journal of the Taiwan Institute of Chemical Engineers (Elsevier)

https://www.journals.elsevier.com/journal-of-the-taiwan-institute-of-chemical-engineers

Impact Factor: 4.794

Accepted April 28th 2021

NONLINEAR NANOFLUID FLUID FLOW UNDER THE CONSEQUENCES OF LORENTZ FORCES AND ARRHENIUS KINETICS THROUGH A PERMEABLE SURFACE: A ROBUST SPECTRAL APPROACH

L. Zhang[1], M. M. Bhatti[1,*], A. Shahid[2], R. Ellahi[3], O. Anwar Bég[4], Sadiq M. Sait[5]

[1] *College of Mathematics and Systems Science, Shandong University of Science & Technology, Qingdao 266590, Shandong People's Republic of* ***China***

[2]*College of Astronautics, Nanjing University of Aeronautics & Astronautics, 210016 Nanjing,* ***China***

[3] *Department of Mathematics and Statistics, International Islamic University, Islamabad,* ***Pakistan***

[4]*Multi-Physical Engineering Sciences, Aeronautical and Mechanical Engineering, School of Science, Engineering and Environment (SEE), The Crescent, Salford, M54WT, England,* ***UK***

[5]*Center for Communications and IT Research, Research Institute, King Fahd University of Petroleum & Minerals, Dhahran 31261,* ***Saudi Arabia***

**Corresponding author: mmbhatti@sdust.edu.cn; mubashirme@yahoo.com*

ABSTRACT:

Background: Emerging applications in nanomaterials processing are increasingly featuring multiple physical phenomena including magnetic body forces, chemical reactions and high temperature behavior. Stimulated by developing a deeper insight of nanoscale fluid dynamics in such manufacturing systems, in the current article, we study the magnetic nanofluid dynamics along a nonlinear porous stretching sheet with Arrhenius chemical kinetics and wall transpiration. Appropriate similarity transformations are employed to simplify the governing flow problem.

Methods: The emerging momentum, thermal energy and nanoparticle concentration ordinary differential conservation equations are solved numerically with a hybrid technique combining Successive Linearization and Chebyshev Spectral Collocation. A parametric study of the impacts of magnetic parameter, porous media parameter, Brownian motion parameter, parameters for thermophoresis, radiation, Arrhenius function, suction/injection (transpiration) and nonlinear stretching in addition to Schmidt number on velocity, temperature and nanoparticle (concentration) distribution is conducted. A detail numerical comparison is presented with different numerical and

analytical techniques as a specific case of the current investigation.

Findings: Increasing chemical reaction constant parameter significantly decreases nanoparticle concentration magnitudes and results in a thickening of the nanoparticle concentration boundary layer. Enhancing the values of activation energy parameter significantly increases the nanoparticle concentration magnitudes. Increasing thermophoresis parameter elevates both temperature and nanoparticle concentration. Increasing radiation parameter increases temperature and thermal boundary layer thickness. Enlarging Brownian motion parameter (smaller nanoparticles) and Schmidt number both depress the nanoparticle concentration.

KEYWORDS: *Magnetic field; Activation energy; Nanofluid; Hybrid Chebyshev spectral solution; Radiation.*

NOMENCLATURE

x, y	Cartesian coordinate system
a	Constant
n	Nonlinear stretching parameter
$B(x)$	Magnetic field
$\bar{k}(x)$	Permeability
$\tilde{u}, \tilde{v}$	Velocity constituents
$\tilde{C}$	Nanoparticle concentration
D_T	Thermophoretic diffusion coefficient
D_B	Brownian-diffusion coefficient
c	Specific heat
$\tilde{t}$	Time

$\overline{K}$	Boltzmann constant
E_a	Activation energy
R_d	Thermal radiation parameter
M	Magnetic parameter
N_b	Brownian motion parameter
N_t	Thermophoresis parameter
S_c	Schmidt number
f_w	Transpiration parameter
Nu_r	Nusselt number
Sh_r	Sherwood number
P_r	Prandtl number

Greek Letters

α	Shrinking/stretching parameter
θ	Dimensionless temperature function
Φ	Dimensionless nanoparticle concentration
ω	Chemical reaction constant
δ	Temperature difference parameter
μ	Dynamic viscosity
ρ	Density
σ	Electrical conductivity
$\bar{\alpha}_m$	Thermal diffusivity

$\bar{\sigma}$	Stefan-Boltzmann constant
k'	Mean absorption coefficient

1.INTRODUCTION

In 1995, Choi [1] introduced the word “nanofluid” to describe a suspension of nanometer-sized particles e.g. copper, silver, aluminum and titanium, having diameters of typically 50nm dispersed in base fluids e.g. ethylene glycol, oil, water and toluene. Nanofluids are therefore a subset of molecular fluids operating at the nanoscale. They have stimulated strong interest in engineering sciences owing to their thermally-enhancing properties. Nanofluid mechanics also provides a robust bridge between bulk materials and molecular or atomic structures. Choi [1] has shown experimentally that nanofluids are stable as long as the size of the nanoparticles is about 100nm. Nanofluids modify base fluid thermal conductivity and can therefore be used to achieve enhanced cooling in for example automobile engine and electronic circuits. Other applications include aerospace propellants (rocket fuels) and energy generation. In parallel with experimental investigations, mathematical and numerical simulations of nanofluid flows have flourished in recent years. Electromagnetic nanofluids which may be manipulated by magnetic or electrical fields have also stimulated some interest owing to growing applications in electrical power [2],

energy systems [3], enhanced oil recovery systems [4] and materials processing [5]. Bég *et al.* [6] investigated transient magnetic nanofluid boundary layer convection from an exponentially stretching sheet embedded in permeable material. Maskaniyan *et al*. [7] used a Eulerian-Lagrangian model and a two-way coupling mechanism for particle movement with multiple sizes through a channel. Bovand *et al.* [8] studied the impact of reflecting and trapped particle boundary conditions on the peristaltic movement with heat transfer through a duct using the Eulerian-Lagrangian model. These studies considered a variety of nanoparticles [9] including titanium oxide, copper oxide, silver oxide and aluminum oxide. Many of these studies have also addressed the stretching sheet problem which is fundamental to materials synthesis. Such flows also arise in coating applications, in which novel nanomaterials can be used to provide enhanced protection and deploy anti-corrosion features and self-healing properties to, for example, steel structures in extreme environments. Further studies on nanofluid transport for different geometrical configurations using various fluids can be found from the references [10-12].

In many *high temperature* materials processing systems, thermal radiation also performs a significant role. The impact of radiation also becomes more prominent when the difference between ambient and surface temperature is high. Bhatti *et al*. [13] scrutinized numerically the influence of thermal radiation and magnetic field on Carreau nanofluid from a shrinkable surface with entropy generation, employing Successive linearization and Chebyshev spectral collocation methods. Laxmi and Shankar [14] explored the impact of nonlinear thermal radiation on boundary layer flow of a Newtonian nanofluid towards shrinking/stretched surfaces with suction/injection. Sohail *et al.* [15] studied entropy generation in three-dimensional swimming of microorganisms in a nanofluid under thermal radiation effects. Waqas *et al*. [16] used Darcy–Forchheimer model to examine the thermal radiation effects on the movement of microorganisms and nanoparticles in

flow propagating through an elastic plate/cylinder with Wu slip effects. Raza *et al*. [17] discussed the thermal radiation effects on convective flow of a Williamson fluid from an elastic curved surface.

The study of magnetohydrodynamics (MHD) i.e. the interaction of electrically conducting fluids and magnetic fields, features in many fields of engineering sciences including cooling of nuclear reactors, the control of boundaries in crystal growth, smart lubrication technology, MHD power generators and MHD sensors etc. Furthermore, the effects of magnetic field on the nanofluid flow are also important in applied physics, medical science and engineering. Ibrahim and Shankar [18] computed the magnetoconvective nanofluid boundary layer flow with momentum, thermal and solutal slip boundary conditions from a permeable stretchable plate. Ibrahim *et al.* [19] considered the MHD effects on stagnation point flow of a nanofluid from a stretched plate. MHD boundary layer nanofluid flow with heat transfer towards a nonlinear stretched surface was analyzed by Mabood *et al.* [20]. A few other relevant works are available in references [21-23].

A porous medium comprises of solid material fibers interspersed with pores. The enhanced internal surface area has numerous advantages in insulation systems, thermal power technologies etc. The increased dissipation area of porous media, for example, achieves improved heat convection compared with conventional solid fins. Moreover, the tortuosity of porous media also makes them ideal for filtration and damping of flows. Low speed porous medium transport is conventionally simulated with the Darcy model [24]. Recent studies have shown that nanofluids permeating porous media achieve enhanced thermal features, such as improved convective heat transfer coefficients and higher thermal conductivity compared to the base material [25].

Hence, nanofluid transport in porous media is attractive from the viewpoint of enhancing the heat transfer characteristics. Recent implementation of nanofluids in porous media includes

vehicle cooling, electronic heat dissipation, transformer temperature control, lubricants and oil [26]. Further studies of nanofluids in a range of technologies are documented in [27-31].

The activation energy terminology, which states as *the nominal supply of energy acquired to induct a chemical reaction*," was established by a Swedish scientist 'Svante Arrhenius' in 1889. Several procedures that include transferal of mass with activation energy are oil container engineering, food production, synthetical processing, oil coating, etc. There are dynamic devices through which chemical reactants are implicated for activating reactions to produce a vast output. Hamid *et al.* [32] scrutinized the influence of activation energy on time-dependent magneto-Williamson nanofluid flow. Zeeshan *et al.* [33] analyzed the assessment of activation energy in Couette-Poiseuille nanofluid flow with chemical reactions and convectively boundary conditions. Khan *et al.* [34] elaborated on activation energy in the Carreau-Yasuda nanomaterials transport with entropy generation in porous media. Chu *et al.* [35] investigated the impact of activation energy on bio-convection magnetohydrodynamic flow of third-grade fluid over a stretched subsurface. Further inquiries on activation energy are available in [36-38].

Inspired by the above inquiries, the objective of the current study is to analyze the MHD nanofluid dynamics with thermal radiation and chemical reaction from a nonlinear perforated stretched sheet. The governing nanofluid conservation equations are transformed with appropriate similarity variables. A magnetic body force is incorporated. The successive linearization method (SLM) combined with the Chebyshev spectral collocation method is employed to obtain accurate solutions of the resulting highly nonlinear, coupled, multi-degree ordinary differential equations, subject to physically viable boundary conditions. The present solutions are compared with former published results from the technical literature and very good correlation is accomplished affirming the validation of the present technique. Furthermore, the physical influence of the emerging

parametric quantities on momentum, heat and mass (nanoparticle concentration) transfer characteristics is studied in detail.

2.MATHEMATICAL MODEL

Incompressible, steady, laminar boundary layer nanofluid flow with constant density from a vertical porous stretching sheet adjacent to an isotropic, homogenous porous medium is considered. The sheet extends with a velocity $u_w = ax^n$ from a fixed origin as shown in **Fig. 1,** where $n \geq 0$ is a nonlinear stretching parameter and $a > 0$ is a constant. Constant temperature and nanoparticle concentration wall conditions are imposed at the stretching sheet i.e., $\tilde{T}_w$ and $\tilde{C}_w$ and these values are higher than the ambient temperature and concentration $\tilde{T}_\infty$ and $\tilde{C}_\infty$. The wall conditions are thus simulated as isothermal and iso-solutal while the buoyancy force, pressure gradient and edge effects are neglected.

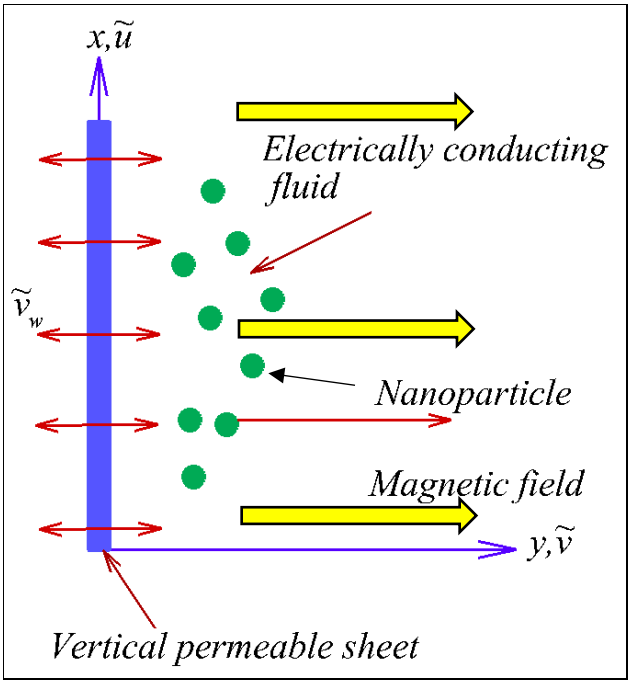

Fig. 1. Geometry of the flow over a vertical permeable sheet under magnetic forces.

An external, varying magnetic field presumed in the mode of $B(x) = B_0 x^{(n-1)/2}$ is enforced here and the induced magnetic field is omitted owing to small magnetic Reynolds number. A variable permeability of the form $\bar{k}(x) = k_0 x^{(1-n)}$ is considered [39-40]. A uni-directional radiative flux acts transverse to the sheet and the nanofluid is presumed to be optically thick. The governing flow equations for mass, momentum, energy (heat) and nanoparticle species concentration conservation, may be formulated, based on amalgamating models from previous studies [41-42] as:

$$\frac{\partial \tilde{u}}{\partial x} + \frac{\partial \tilde{v}}{\partial y} = 0, \tag{1}$$

$$\tilde{u}\frac{\partial \tilde{u}}{\partial x} + \tilde{v}\frac{\partial \tilde{v}}{\partial y} = \frac{\mu}{\rho}\frac{\partial^2 \tilde{u}}{\partial y^2} - \frac{\mu}{\rho \bar{k}(x)}\tilde{u} + \frac{-\sigma B_0^2(x)}{\rho}\tilde{u}, \tag{2}$$

$$\tilde{u}\frac{\partial \tilde{T}}{\partial x} + \tilde{v}\frac{\partial \tilde{T}}{\partial y} = \bar{\alpha}_m \frac{\partial^2 \tilde{T}}{\partial y^2} + \tau\left[D_B \frac{\partial \tilde{T}}{\partial y}\frac{\partial \tilde{C}}{\partial y} + \frac{D_T}{\tilde{T}_\infty}\left(\frac{\partial \tilde{T}}{\partial y}\right)^2\right] - \frac{1}{\rho c_p}\frac{\partial \bar{Q}_r}{\partial y}, \tag{3}$$

$$\tilde{u}\frac{\partial \tilde{C}}{\partial x} + \tilde{v}\frac{\partial \tilde{C}}{\partial y} = D_B \frac{\partial^2 \tilde{C}}{\partial y^2} + \frac{D_T}{\tilde{T}_\infty}\frac{\partial^2 \tilde{C}}{\partial y^2} - {k_r}^2\left(\tilde{C} - \tilde{C}_\infty\right)\left(\frac{\tilde{T}}{\tilde{T}_\infty}\right)^m \exp\left(\frac{-E_a}{\overline{K}\tilde{T}}\right), \tag{1}$$

In the above equations $\tilde{u}, \tilde{v}$ are the velocity components, *x, y* are Cartesian coordinates, $\tilde{t}$ is time, $\tilde{C}$ is a nanoparticle concentration, D_T is a thermophoretic diffusion coefficient, D_B is a Brownian-diffusion coefficient, $\bar{\alpha}_m = \kappa/(\rho c)_f$ is a thermal diffusivity, c is a specific heat, $\tau = (\rho c)_p/(\rho c)_f$ the ratio betwixt the effective heat capacity of the nanoparticles and heat capacity of the base fluid, μ is a viscosity of nanofluid, ρ is density of the fluid and σ is electrical conductivity. Furthermore, in Eqn. (4) the term $\left(\frac{\tilde{T}}{\tilde{T}_\infty}\right)^m \exp\left(\frac{-E_a}{K\tilde{T}}\right)$ represents the modified form of the Arrhenius function, $\overline{K} = 8.61 \times 10^{-5} eV/K$ denotes the Boltzmann constant, m denotes the unitless exponent fitted rate constant having range $-1 < m < 1$ and E_a denotes the activation energy [43].

The applied boundary conditions take the form:

$$\tilde{u} = u_w(x) = ax^n, \tilde{v} = \tilde{v}_w, \tilde{T} = \tilde{T}_w, \tilde{C} = \tilde{C}_w \text{ at } y = 0, \tag{5}$$

$$\tilde{u} \to 0, \tilde{T} = \tilde{T}_\infty, \tilde{C} = \tilde{C}_\infty \text{ at } y \to \infty. \tag{6}$$

The nonlinear radiative heat flux is described as:

$$\bar{Q}_r = -\frac{4\bar{\sigma}}{3k'}\frac{\partial \tilde{T}^4}{\partial y} = -\frac{16\bar{\sigma}\tilde{T}_\infty^{\,3}}{3k'}\frac{\partial \tilde{T}}{\partial y}. \tag{7}$$

Where $\bar{\sigma}$ denotes the Stefan-Boltzmann constant and k' is the mean absorption coefficient.

It is judicious to invoke the following similarity transformation and dimensionless variables:

$$\eta = \sqrt{\frac{(n+1)a}{2\nu}}\, x^{\frac{n-1}{2}} y, u = ax^n f'(\eta), \tilde{v} = -\sqrt{\frac{a\nu(1+n)}{2}}\, x^{\frac{n-1}{2}}\left[f + \left(\frac{n-1}{n+1}\right)\eta f'\right], \tag{8}$$

Using Eqns. (7)-(8) in Eqns. (2) to (6), the following ordinary differential equations emerge:

$$f''' - \frac{2n}{n+1}f'^2 + ff'' - Mf' - kf' = 0, \tag{9}$$

$$\left(\frac{1}{P_r} + \frac{4}{3}R_d\right)\theta'' + f\theta' + N_b\theta'\Phi' + N_t\theta'^2 = 0, \tag{10}$$

$$\Phi'' + \frac{1}{2}S_c f\Phi' + \frac{N_t}{N_b}\theta'' - S_c\omega(1+\delta\theta)^m e^{\left(\frac{-E}{1+\delta\theta}\right)}\Phi = 0. \tag{11}$$

The respective transformed boundary conditions are:

$$f(0) = f_w, f'(0) = \alpha, f'(\infty) = 0, \tag{12}$$

$$\theta(0) = 1, \theta(\infty) = 0, \Phi(0) = 1, \Phi(\infty) = 0. \tag{13}$$

Where

$$M=\frac{2B_0^2\sigma}{\rho a(n+1)},\theta=\frac{\tilde{T}-\tilde{T}_\infty}{\tilde{T}_w-\tilde{T}_\infty},P_r=\frac{\nu}{\overline{\alpha}_m},\ \Phi=\frac{\tilde{C}-\tilde{C}_\infty}{\tilde{C}_w-\tilde{C}_\infty},k=\frac{2\nu}{(n+1)ak_0},R_d=\frac{4\overline{\sigma}\tilde{T}_\infty^{\,3}}{\mu c_p k'},N_b=\frac{(\rho c)_p}{(\rho c)_f\nu}D_B\left(\tilde{C}_w-\tilde{C}_\infty\right),N_t=\frac{(\rho c)_p D_T(\tilde{T}_w-\tilde{T}_\infty)}{(\rho c)_f\nu\tilde{T}_\infty},S_c=\frac{\nu}{D_B},f_w=-\frac{v_w}{\left(\sqrt{\frac{a\nu(n+1)}{2}}x^{\frac{n-1}{2}}\right)},\omega=\frac{2k_r^{\,2}}{a(n+1)x^{n-1}},\delta=\frac{(T_w-T_\infty)}{T_\infty},E=\frac{E_a}{\overline{K}T_\infty}. \quad (14)$$

In the above equation, α the shrinking/stretching parameter, M is a magnetic interaction parameter, θ is temperature function, P_r is Prandtl number, Φ is nanoparticle concentration, k is a permeability parameter, R_d is a thermal radiation parameter, N_b is the Brownian motion parameter, N_t the thermophoresis parameter, S_c the Schmidt number, f_w is a transpiration parameter, ω the chemical reaction constant, δ the temperature difference parameter, and E denotes the activation energy parameter. It is noteworthy that the above results can be reduced to the *constant velocity sheet (moving plate) case* by taking $n=0$ as a special case. The physical quantities of significance i.e., *local Nusselt number* (dimensionless heat transfer rate to the wall) and *Sherwood number* (dimensionless nanoparticle mass transfer rate to the wall) are described in non-dimensional form respectively by:

$$Nu_r=-\left(1+\frac{4}{3}R_d\right)\theta'(0),Sh_r=-\Phi'(0). \quad (15)$$

Here Nu_r and Sh_r denote the dimensionless Nusselt number and Sherwood number.

3.SOLUTION TECHNIQUE

Employing the successive linearization method (SLM) over Eqn. (9) alongside the boundary conditions (12), we set [9]:

$$f(\eta)=f_I(\eta)+\sum_{N=0}^{I-1}f_N(\eta),\ (I=1,2,3,\dots), \quad (16)$$

where f_I are functions to be determined and achieved through iterations by resolving the linearized

form of Eq. (9), and presuming that f_I $(0 \leq N \leq I-1)$ are known from preceding iterations. The scheme operates with an initially approximated function f_0, which satisfies the boundary conditions in Eqn. (12) by virtue of the SLLM technique. The appropriate starting assumption of the governing equation is:

$$f_0 = \alpha - 1 + \frac{1-\alpha}{e^{\eta}} + \eta + f_w. \tag{17}$$

By writing Eqn. (9) in general mode we have:

$$\boldsymbol{\mathcal{L}}(f, f', f'', f''') + \boldsymbol{\mathcal{N}}(f, f', f'', f''') = 0, . \tag{18}$$

where

$$\boldsymbol{\mathcal{L}}(f, f', f'', f''') = f''', \tag{19}$$

and

$$\boldsymbol{\mathcal{N}}(f, f', f'', f''') = ff'' - \frac{2n}{n+1} f'^2 - Mf' - kf', \tag{20}$$

Here $\boldsymbol{\mathcal{L}}$ and $\boldsymbol{\mathcal{N}}$ designate the *linear* and *non-linear* factors in Eqn. (9). Replacing Eqn. (18) in Eqn. (9) and isolating the linear components, yields:

$$f_I''' + \mathcal{B}_{0,I-1} f_I''' + \mathcal{B}_{1,I-1} f_I'' + \mathcal{B}_{2,I-1} f_I' + \mathcal{B}_{3,I-1} f_I = \mathbf{r}_{I-1}, \tag{21}$$

The associated boundary conditions are transformed into:

$$f_I(0) = 0, f_I'(0) = 0, f_I'(\infty) = 0. \tag{22}$$

Now, Eqn. (21) is solved through a numerical technique known as the Chebyshev spectral collocation method [44-45]. Instantly, to implement this technique numerically, the physical portion $[0, \infty)$ is shortened to $[0, \Gamma]$ by taking Γ to be of reasonable extent. The following transmutation to this portion, is applied beyond $[-1,1]$, leading to:

$$\Omega = -1 + \frac{2\eta}{\Gamma}. \tag{23}$$

The subsequent discretization is contemplated in $[-1,1]$ by applying *Gauss-Lobatto* collocation points to describe the nodes in $[-1,1]$ as:

$$\Omega_J = \cos\frac{\pi J}{N},\ (J = 0,1,2,3 \dots N), \tag{24}$$

having $(N+1)$ number of collocation points. The Chebyshev spectral collocation method is founded upon the notion of a differentiation matrix $\mathbf{D}$ that maps a vector of the function values $= [f(\Omega_0), \dots, f(\Omega_N)]^{\boldsymbol{T}}$. These collocation points for a vector $\mathbf{G}'$ are then prescribed as:

$$\mathbf{G}' = \sum_{K=0}^{N} \mathbf{D}_{KJ} f(\Omega_K) = \mathbf{DG}, \tag{25}$$

The differential of the p-th order of the function $f(\Omega)$ is defined as follows:

$$f^p(\Omega) = \mathbf{D}^p\mathbf{G}. \tag{26}$$

The elements of matrix $\mathbf{D}$ may be determined through the mechanism suggested by Trefethen [46]. At this stage, employing the spectral method, alongside differential matrices on the linearized modes Eqns. (21)-(22), generates the *linearized* matrix system as:

$$\mathbf{A}_{I-1}\mathbf{G}_I = \mathbf{R}_{I-1}, \tag{27}$$

The boundary conditions now emerge as:

$$f_I(\Omega_N) = 0, \sum_{K=0}^{N} \mathbf{D}_{NK} f_I(\Omega_K) = 0, \sum_{K=0}^{N} \mathbf{D}_{\mathbf{0}K} f_I(\Omega_K) = 0, \sum_{K=0}^{N} \mathbf{D}_{\mathbf{0}K}^{\mathbf{2}} f_I(\Omega_K) = 0, \tag{28}$$

Where

$$\mathbf{A}_{I-1} = \mathbf{D^3} + \mathcal{B}_{0,I-1}\mathbf{D^3} + \mathcal{B}_{1,I-1}\mathbf{D^2} + \mathcal{B}_{2,I-1}\mathbf{D} + \mathcal{B}_{3,I-1}. \quad (29)$$

In this equation, $\mathcal{B}_{s,I-1}(s = 0,1,\dots 3)$ are $(N+1)\times(N+1)$ diagonal matrices along with $\mathcal{B}_{s,I-1}(\Omega_J)$ on the *principal diagonal*.

$$\mathbf{G}_I = f_I(\Omega_J), \mathbf{R}_I = \mathbf{r}_I(\Omega_J).\ (J = 0,1,2,3,\dots N). \quad (30)$$

Following subsequent operation on Eq. (29), the outcomes of f_I are attained through performing iterations on Eqn. (29). Formally the solution for $f(\eta)$ is achieved from Eq. (29). As Eqns. (10)-(11) are *linear* now thence, by employing Chebyshev pseudo-spectral method successively one attains:

$$\boldsymbol{\mathcal{R}}\mathbf{H} = \mathbf{S}, \quad (31)$$

The corresponding boundary conditions emerge as:

$$\theta(\Omega_N) = 1, \theta(\Omega_0) = 0, \quad (32)$$

$$\Phi(\Omega_N) = 1, \Phi(\Omega_0) = 0, \quad (33)$$

Here $\mathbf{H} = \left(\theta(\Omega_J), \Phi(\Omega_J)\right)$, $\boldsymbol{\mathcal{R}}$ is the system of linear coupled equations, $\boldsymbol{S}$ is a vector of zeros, and all vectors in Eqn. (32) are reformed to a diagonal matrix. The final stage involves imposing the boundary conditions in Eqns. (32)-(33) over the first and last rows of $\boldsymbol{\mathcal{R}}$ and $\mathbf{S}$, subsequently.

4.RESULTS AND DISCUSSION

Large-scale computations are performed for the effects of the key thermophysical parametric quantities on the nanofluid heat, mass and momentum characteristics. In particular we focus on the evolution of velocity distribution, temperature distribution and nanoparticle concentration with magnetic parameter *M*, permeability parameter *k*, stretching parametric

quantity n, Prandtl number P_r, Brownian motion parameter N_b, thermophoresis parameter N_t, radiation parameter R_d, Schmidt number S_c, chemical reaction constant ω, temperature difference parameter δ, activation energy parameter E and suction/injection parametric f_w, respectively. For affirming the validation of the current technique, benchmarking against earlier studies [47-49] is included. **Table 1** documents the numerical results for local Nusselt number Nu_x and Sherwood number Sh_r against all appropriate parametric quantities. **Table 2** displays the numerical comparison of velocity distribution f' at different values of transverse coordinate, η. This table shows the numerical comparison with other numerical methods such as the Finite element method (FEM), Finite difference method (FDM) and Homotopy analysis method (HAM). Evidently the results obtained from Successive linearization method are in excellent agreement with all these other methods. It is further emphasized that the Successive linearization method converges more rapidly as compared with FEM, FDM and HAM. **Table 3** shows the comparison for wall skin friction i.e. $-f''(0)$ by fixing $M = k = 0$ as an appropriate case for present inquiry (i.e. the purely fluid infinite permeability, non-magnetic case). **Table 4** represents the numerical comparison of temperature distribution θ at different η locations. This table also shows comparison with other numerical and analytical methods. Again, it is apparent that the current outcomes closely correlate with other methods, and furthermore the present technique converges faster. **Table 5** provides a numerical comparison of dimensionless temperature gradient at the wall i.e. $\theta'(0)$ by taking $M = k = R_d = 0$ as another appropriate special case (i.e. purely fluid, non-magnetic case without radiative flux). From these tables it is evident that the present computations agree closely with previous studies thereby confirming the validity of the current successive linearization technique employed.

Fig. (2) to **(7)** illustrate velocity, temperature and nanoparticle concentration distribution

respectively with prescribed parametric values [49]: $f_w = 0.5; n = 2;\ M = 1; k = 0.5; N_b = 0.2; N_t = 0.2; R_d = 0.5; P_r = 6; \omega = 1; S_c = 5.$

Fig. (2) together with Fig. (3) shows the velocity distribution with increment in permeability parameter value *k*, magnetic parameter *M*, stretching parametric value *n* and suction/injection parametric value f_w. Fig. (2) illustrates that by enlarging the permeability parametric value, the velocity of the fluid decelerates significantly. Although the Darcian body force in the transformed momentum boundary layer Eqn. (9) i.e. -$kf^{/}$ is directly proportional to parameter, *k*, this parameter is in fact a reciprocal of the actual permeability of the porous medium (k_o) i.e. $k = \frac{2\nu}{(n+1)ak_0}$, as per the definition in Eqn. (8). Therefore, increasing k values imply a decrease in ko values and a depletion in permeability. Physically this corresponds to greater density of solid fibers in the porous matrix which produces greater Darcian resistance to the percolating nanofluid. This results in an inhibition in momentum diffusion in the regime and an increase in momentum boundary layer thickness. The effects of magnetic interaction parameter (*M*) show a similar influence i.e., stronger magnetic field decelerates the flow and simultaneously enhances momentum (hydrodynamic) boundary layer thickness. Physically, a Lorentz magnetic body force is generated whenever a magnetic field is applied to any conducting fluid. Lorentz force acts transverse to the direction of the magnetic field and provides a significant resistance to the fluid which damps the flow. Fig. (3) demonstrates that an increment in suction parameter f_w leads a notable reduction in the velocity profile, since the boundary layer is drawn more towards the sheet surface and this destroys momentum. Increasing magnetic field and suction therefore both *enhance* the momentum i.e., hydrodynamic boundary layer thickness, as does an elevation in permeability parameter. In all cases no backflow is computed i.e. positive velocities are computed throughout the boundary layer transverse to the wall.

Fig. (4) and Fig. (5) depict temperature distribution for diverse values of N_b, N_t, P_r and R_d. Fig. (4) portrays that by enlarging Brownian motion parameter N_b, temperature magnitudes are boosted. Brownian motion is the movement of tiny particles within the fluid and the nanoparticles therefore collide and interact. Higher numerical values in N_b correspond to small sized nanoparticles, which enhances thermal conduction via increased surface area, and this also enhances temperatures and thermal boundary layer thickness. Increment in thermophoresis parameter N_t tends to increase the temperature profile also as shown in Fig. (4) since it encourages migration of nanoparticles through the boundary layer under the action of a temperature gradient. This trend is sustained across the boundary layer. Fig. (5) implies that an increment in thermal radiation parameter R_d accentuates the temperature magnitudes very significantly. Thermal radiative flux stimulates the flow i.e. energizes the transport and this also manifests in a thickening of the thermal boundary layer. Increasing Prandtl number P_r, reduces magnitudes of temperature since larger Prandtl number P_r is associated with reduced thermal conductivity. Thermal boundary layer thickness is thus diminished with larger Prandtl number.

Fig. (6) and Fig. (7) illustrate the variation in nanoparticle concentration with N_b, N_t, S_c and γ. Inspection of Fig. (6), reveals that higher values of Brownian-motion parameter N_b and thermophoresis parameter N_t *respectively reduce and increase* the nanoparticle concentration values i.e. they respectively *decrease and increase* concentration boundary layer thickness. This is the opposite behavior to that experienced by the temperature. Fig. (7) that increasing chemical reaction constant ω and Schmidt number S_c both induce substantial reduction in the nanoparticle concentration distribution and an associated thickening of the nanoparticle species boundary layer. With increasing ω more nanoparticles are transformed chemically and this results in a reduction in the original nanoparticle species. Larger Schmidt number implies a smaller species diffusivity

of nanoparticles which inhibits mass diffusion into the boundary layer and effectively decreases nanoparticle concentration values. Fig. (8) is plotted to determine the impact of temperature difference parameter δ and activation energy parameter E on nanoparticle concentration field. With enhancing the values of activation energy parameter E, it is noticed that the concentration distributed rises significantly (leading also to a thicker concentration boundary layer). However, the temperature difference parameter δ depletes the concentration magnitudes and produces a thinner concentration boundary layer.

Table 1: Numerical values for Nusselt number and Sherwood number with variation in $P_r, R_d, \gamma, N_b, S_c$ and N_t at $n = 2$.

P_r	N_b	N_t	R_d	S_c	E	δ	ω	m	Nu_r	Sh_r
3	0.5	0.1	0.4	3	1	1	1	0.5	0.915294	2.96106
5									0.978465	2.95214
7									1.00843	2.94773
	0.4								1.00249	2.94164
	0.6								0.834918	2.97425
	0.7								0.76093	2.98387
		0.3							0.827984	2.94929
		0.4							0.788169	2.95203
		0.5							0.750705	2.95948
			0.2						0.868026	2.94126
			0.5						0.936263	2.96832
			0.6						0.957441	2.97427

				1					1.07325	0.992931
				1.5					1.02815	1.31109
				2.5					0.974811	1.85345
					0.3				0.939006	2.41126
					0.6				0.946934	2.26878
					0.9				0.954904	2.13733
						0.3			0.971274	1.826
						0.6			0.964799	1.95083
						0.9			0.959234	2.06166
							0.2		1.00866	1.37471
							0.6		0.977447	1.77681
							0.9		0.961853	2.0215
								-0.5	0.974545	1.75164
								0	0.966522	1.90448
								0.4	0.959419	2.05413

Table 2: Comparability for $f'(0)$ with earlier studies for $M = k = 0$.

η	FEM [47]	FDM [47]	HAM [48]	SLM (Present results)
0.0	1.0000	1.0000	1.0000	1.000000
1.0	0.3479	0.3459	0.3483	0.347896
2.0	0.1270	0.1210	0.1281	0.127006
3.0	0.0464	0.0464	0.0481	0.046428
4.0	0.0161	0.0160	0.0182	0.016068

5.0	0.0045	0.0043	0.0069	0.004464
6.0	0.0000	0.0000	0.0026	0.000000

Table 3: Numerical comparison of $-f''(0)$ with earlier studies for $M = k = 0$.

n	Cortell [49]	Rashidi et al. [48]	SLM (Present results)
0	0.6275	0.6275	0.627547
0.5	0.8894	0.8894	0.889477
0.75	0.9537	0.9537	0.953786
1.0	1.0	1.0	1.000000
1.5	1.0615	1.0615	1.061587
3.0	1.1485	1.1485	1.148588
7.0	1.2168	1.2168	1.216847

Table 4: Numerical comparison of $\theta(0)$ with earlier studies for $M = R_d = k = 0$.

η	FEM [47]	FDM [47]	HAM [48]	SLM (Present results)
0.0	1.0000	1.0000	1.0000	1.000000
1.0	0.5016	0.4916	0.4717	0.473756
2.0	0.1417	0.1410	0.1384	0.139701
3.0	0.0271	0.0270	0.0289	0.029314
4.0	0.0043	0.0041	0.0049	0.004964
5.0	0.0006	0.0006	0.0007	0.000679
6.0	0.0000	0.0000	0.0001	0.000000

Table 5: Numerical comparison of $-\theta'(0)$ with earlier studies for $M = R_d = k = 0$.

n	Cortell [49]	Rashidi et al. [48]	SLM (Present results)
0.2	0.6102	0.6102	0.6102
0.5	0.5952	0.5952	0.5952
1.5	0.5745	0.5745	0.5745
3.0	0.5644	0.5644	0.5644
10.0	0.5549	0.5549	0.5549

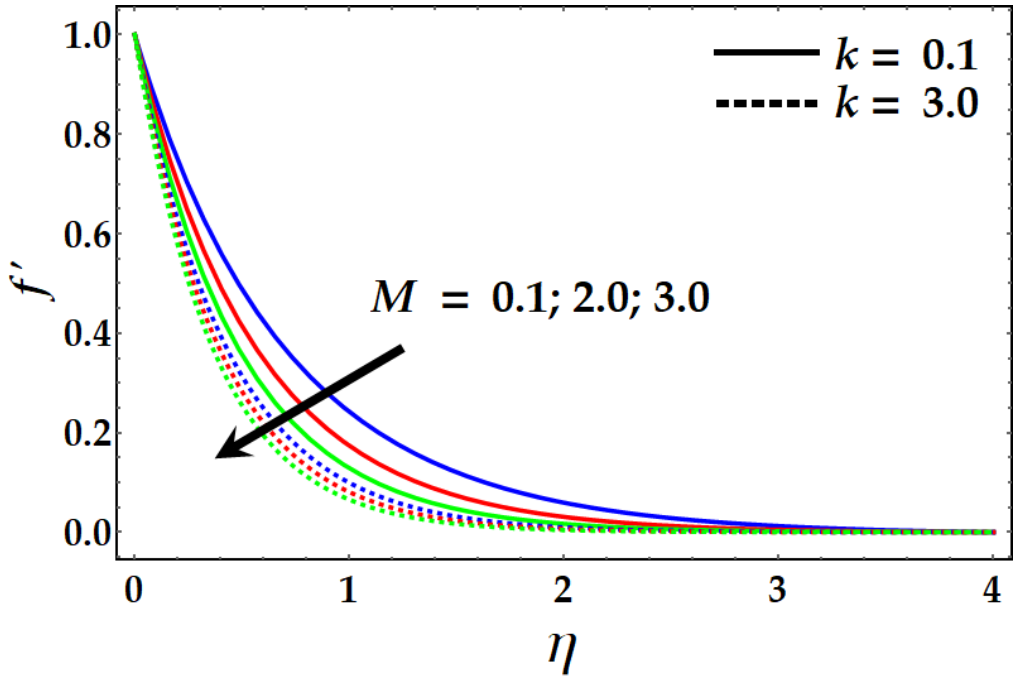

Fig. 2. Velocity distribution for variation in *M* and *k*.

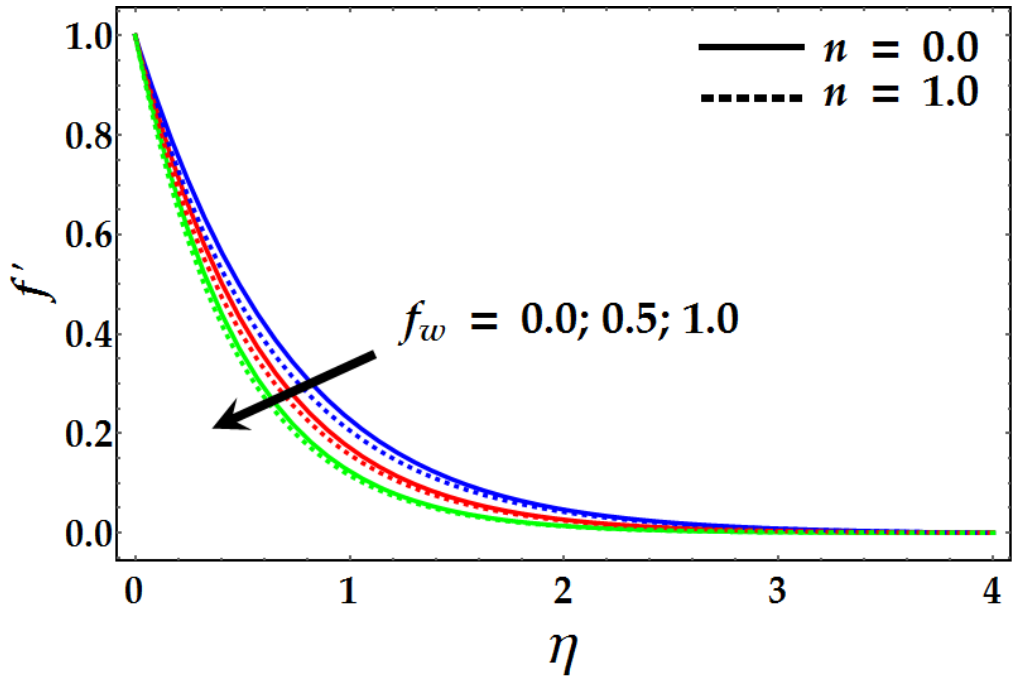

Fig. 3. Velocity distribution for f_w and n.

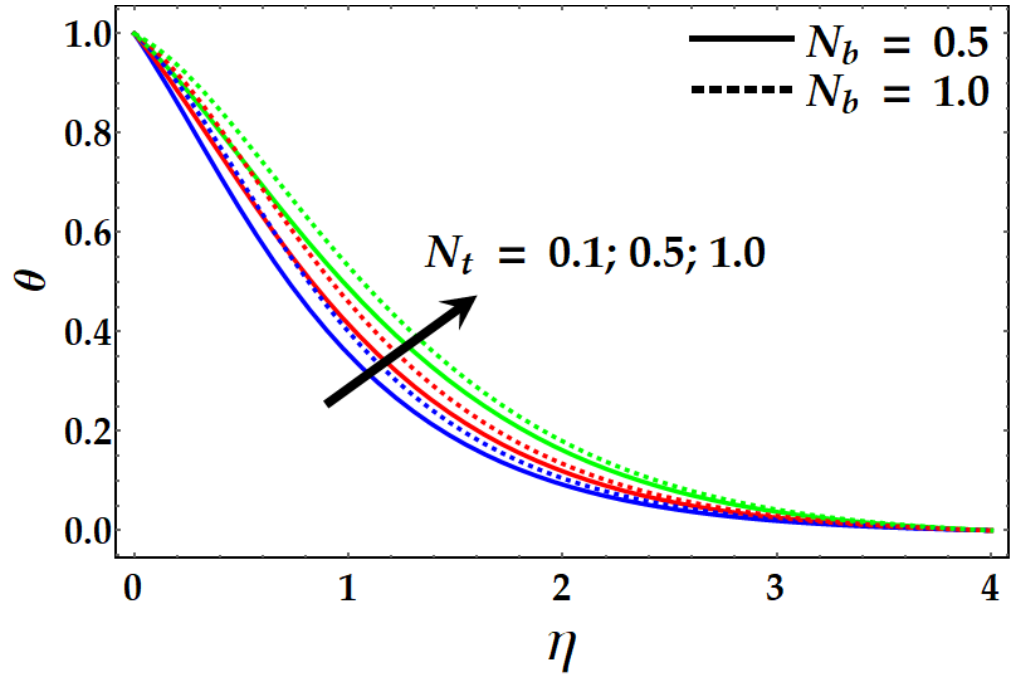

Fig. 4. Temperature distribution for N_t and N_b.

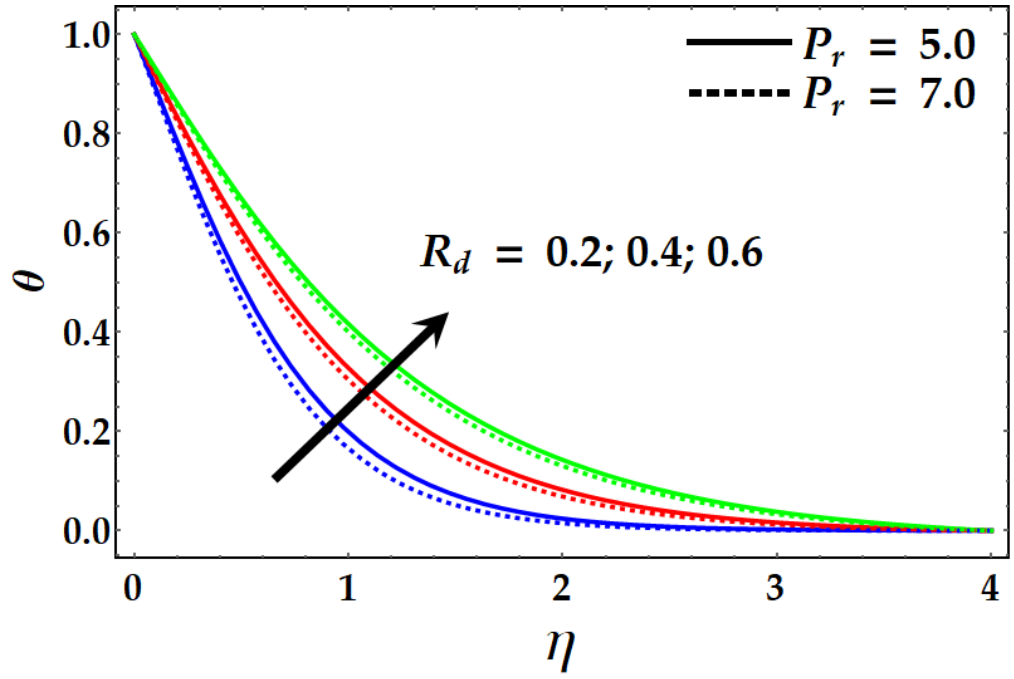

Fig. 5. Temperature distribution for P_r and R_d.

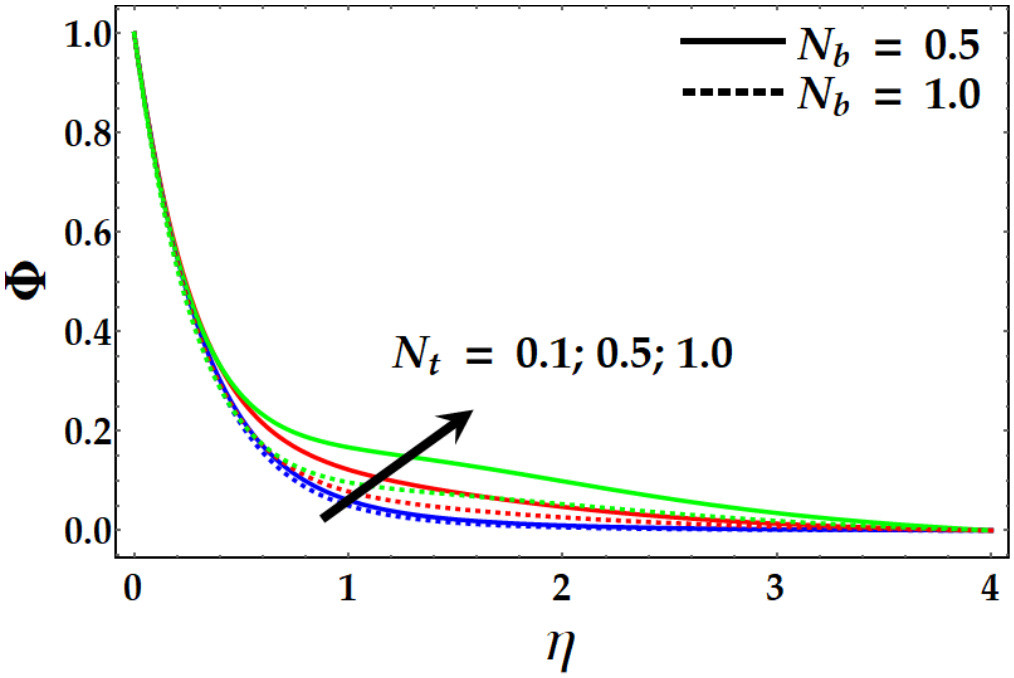

Fig. 6. Concentration distribution for N_b and N_t.

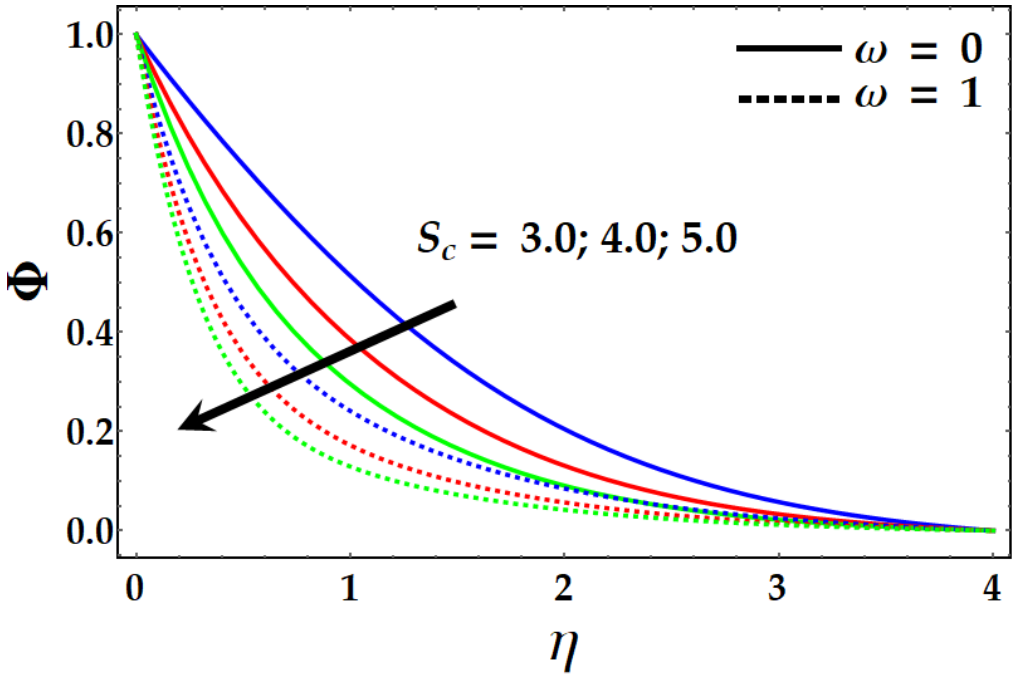

Fig. 7. Concentration distribution for S_c and ω.

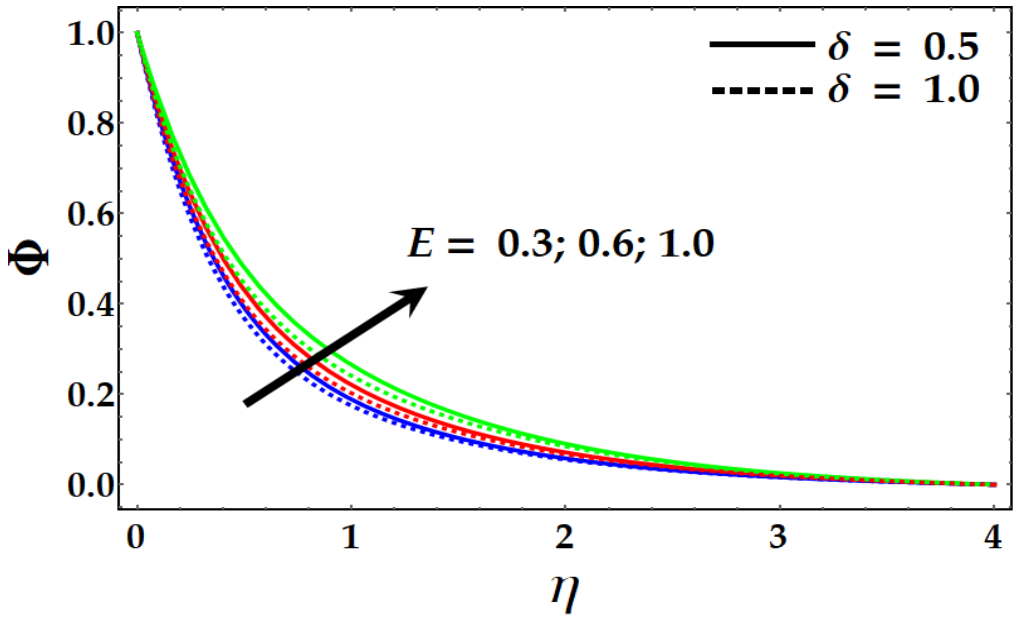

Fig. 8. Concentration distribution for E and δ.

5.CONCLUSIONS

A theoretical and numerical study of magnetohydrodynamic (MHD) nanofluid boundary layer flow from a nonlinear porous stretching sheet adjacent to a porous medium with the effects of activation energy and thermal radiation has been presented. The transformed dimensionless

two-point ordinary differential boundary value problem is solved numerically by combining the Successive Linearization method (SLM) and Chebyshev Spectral Collocation method. The physical effects of emerging pertinent parameters on heat, mass and momentum transfer characteristics is elaborated in detail. Validation of the solutions with some particular cases from the literature is displayed. The key observations from the current simulations may be outlined as follows:

(i) Increasing magnetic field and porous medium drag force parameter tend to diminish the nanofluid velocity distribution and enhance momentum boundary layer thickness.

(ii) An increment in suction parametric value f_w induces strong retardation in the nanofluid flow and also reduces the nanofluid momentum boundary layer thickness.

(iii) Greater thermophoresis parameter enhances both temperature and nanoparticle concentration magnitudes.

(iv) Increasing radiation parameter raises the temperature profile and thermal boundary layer thickness.

(v) Enlarging Brownian-motion parameter enhances temperatures while it depletes nanoparticle concentration values.

(vi) Increasing Schmidt number and chemical reaction constant parameter reduces the nanoparticle concentration magnitudes and concentration boundary layer thickness.

(vii) Enhancing values of activation energy parameter significantly elevate the nanoparticle concentration magnitudes.

(viii) The hybrid successive linearization and Chebyshev spectral method work efficiently for nonlinear nanofluid problems. The current analysis however has been confined to Newtonian reactive magnetized nanofluid flows. Forthcoming work will address non-Newtonian e.g. micropolar [50] and variable viscosity [51] nanofluids and will be communicated soon.

REFERENCES

[1] Choi SU. Enhancing thermal conductivity of fluids with nanoparticles, developments, and applications of non-Newtonian flows, *ASME International Mechanical Engineering Congress and Exposition. American Society of Mechanical Engineering*. 1995.

[2] Segal V, Hjortsberg A, Rabinovich A, Nattrass D, Raj K. AC (60 Hz) and impulse breakdown strength of a colloidal fluid based on transformer oil and magnetite nanoparticles. In *Conference Record of the 1998 IEEE International Symposium on Electrical Insulation (*Cat. No. 98CH36239) 1998 Jun 7 (Vol. 2, pp. 619-622). IEEE.

[3] Jia L, Chen Y, Lei S, Mo S, Luo X, Shao X. External electromagnetic field-aided freezing of CMC-modified graphene/water nanofluid. *Applied Energy*. 2016 Jan 15;1 62:1670-7.

[4] Yahya N, Kashif M, Shafie A, Soleimani H, Zaid HM, Latiff NR. Improved oil recovery by high magnetic flux density subjected to iron oxide nanofluids. In *Journal of Nano Research* 2014 (Vol. 26, pp. 89-99). Trans Tech Publications Ltd.

[5] Nkurikiyimfura I, Wang Y, Pan Z. Heat transfer enhancement by magnetic nanofluids—a review. *Renewable and Sustainable Energy Reviews*. 2013 May 1; 21:548-61.

[6] Bég OA, Khan MS, Karim I, Alam MM, Ferdows M. Explicit numerical study of unsteady hydromagnetic mixed convective nanofluid flow from an exponentially stretching sheet in porous media. *Applied Nanoscience*. 2014 Nov;4(8):943-57.

[7] Maskaniyan M, Rashidi S, Esfahani JA. A two-way couple of Eulerian-Lagrangian model for particle transport with different sizes in an obstructed channel. *Powder Technology*. 2017 May 1; 312:260-9.

[8] Bovand M, Rashidi S, Ahmadi G, Esfahani JA. Effects of trap and reflect particle boundary conditions on particle transport and convective heat transfer for duct flow-A two-way coupling of Eulerian-Lagrangian model. *Applied Thermal Engineering*. 2016 Sep 5; 108:368-77.

[9] Li D, Fang W, Feng Y, Geng Q, Song M. Stability properties of water-based gold and silver nanofluids stabilized by cationic gemini surfactants. *Journal of the Taiwan Institute of Chemical Engineers.* 2019 Apr 1; 97:458-65.

[10] Abumandour RM, Eldesoky IM, Kamel MH, Ahmed MM, Abdelsalam SI. Peristaltic thrusting of a thermal-viscosity nanofluid through a resilient vertical pipe. Zeitschrift für Naturforschung A. 2020 Aug 27;75(8):727-38.

[11] Bhatti MM, Marin M, Zeeshan A, Ellahi R, Abdelsalam SI. Swimming of motile gyrotactic microorganisms and nanoparticles in blood flow through anisotropically tapered arteries. *Frontiers in Physics*. 2020 Apr 8; 8:95.

[12] Sohani A, Shahverdian MH, Sayyaadi H, Samiezadeh S, Doranehgard MH, Nizetic S, Karimi N. Selecting the best nanofluid type for A photovoltaic thermal (PV/T) system based on reliability,

efficiency, energy, economic, and environmental criteria. *Journal of the Taiwan Institute of Chemical Engineers*. 2021 Mar 7.

[13] Bhatti MM, Abbas T, Rashidi MM, Ali ME. Numerical simulation of entropy generation with thermal radiation on MHD Carreau nanofluid towards a shrinking sheet. *Entropy*. 2016 Jun;18(6):200.

[14] Laxmi TV, Shankar B. Effect of nonlinear thermal radiation on boundary layer flow of viscous fluid over nonlinear stretching sheet with injection/suction. *Journal of Applied Mathematics and Physics.* 2016 Feb 17;4(2):307-19.

[15] Sohail M, Naz R, Abdelsalam SI. On the onset of entropy generation for a nanofluid with thermal radiation and gyrotactic microorganisms through 3D flows. *Physica Scripta*. 2020 Feb 11;95(4):045206.

[16] Waqas H, Imran M, Muhammad T, Sait SM, Ellahi R. On bio-convection thermal radiation in Darcy–Forchheimer flow of nanofluid with gyrotactic motile microorganism under Wu's slip over stretching cylinder/plate. *International Journal of Numerical Methods for Heat & Fluid Flow*. 2020 Sep 23.

[17] Raza R, Mabood F, Naz R, Abdelsalam SI. Thermal transport of radiative Williamson fluid over stretchable curved surface. *Thermal Science and Engineering Progress*. 2021 Feb 27:100887.

[18] Ibrahim W, Shankar B. MHD boundary layer flow and heat transfer of a nanofluid past a permeable stretching sheet with velocity, thermal and solutal slip boundary conditions. *Computers & Fluids.* 2013 Apr 20; 75:1-0.

[19] Ibrahim W, Shankar B, Nandeppanavar MM. MHD stagnation point flow and heat transfer due to nanofluid towards a stretching sheet. *International Journal Heat Mass Transfer*. 2013 Jan 1;56(1-2):1-9.

[20] Mabood F, Khan WA, Ismail AM. MHD boundary layer flow and heat transfer of nanofluids over a nonlinear stretching sheet: a numerical study. *Journal of Magnetism and Magnetic Materials*. 2015 Jan 15; 374:569-76.

[21] Rashidi S, Esfahani JA. The effect of magnetic field on instabilities of heat transfer from an obstacle in a channel. *Journal of Magnetism and Magnetic Materials*. 2015 Oct 1; 391:5-11.

[22] Rashidi S, Bovand M, Esfahani JA. Opposition of Magnetohydrodynamic and AL_2O_3–water nanofluid flow around a vertex facing triangular obstacle. *Journal of Molecular Liquids*. 2016 Mar 1; 215:276-84.

[23] Bovand M, Rashidi S, Esfahani JA. Optimum interaction between magnetohydrodynamics and nanofluid for thermal and drag management. *AIAA Journal of Thermophysics and Heat Transfer*. 2017 Jan;31(1):218-29.

[24] Abad JM, Alizadeh R, Fattahi A, Doranehgard MH, Alhajri E, Karimi N. Analysis of transport processes in a reacting flow of hybrid nanofluid around a bluff-body embedded in porous media using artificial neural network and particle swarm optimization. *Journal of Molecular Liquids*. 2020 Sep 1; 313:113492.

[25] Sadeghinezhad E, Mehrali M, Saidur R, Mehrali M, Latibari ST, Akhiani AR, Metselaar HS. A comprehensive review on graphene nanofluids: recent research, development and applications. *Energy Conversion and Management*. 2016 Mar 1; 111:466-87.

[26] Devendiran DK, Amirtham VA. A review on preparation, characterization, properties and applications of nanofluids. *Renewable and Sustainable Energy Reviews*. 2016 Jul 1; 60:21-40.

[27] Rashidi S, Mahian O, Languri EM. Applications of nanofluids in condensing and evaporating systems. *Journal of Thermal Analysis and Calorimetry*. 2018 Mar;131(3):2027-39.

[28] Dogonchi AS, Nayak MK, Karimi N, Chamkha AJ, Ganji DD. Numerical simulation of hydrothermal features of Cu–H_2O nanofluid natural convection within a porous annulus considering diverse configurations of heater. *Journal of Thermal Analysis and Calorimetry*. 2020 Feb 17:1-7.

[29] Nazari S, Ellahi R, Sarafraz MM, Safaei MR, Asgari A, Akbari OA. Numerical study on mixed convection of a non-Newtonian nanofluid with porous media in a two lid-driven square cavity. *Journal of Thermal Analysis and Calorimetry*. 2020 May;140(3):1121-45.

[30] Siavashi M, Bozorg MV, Toosi MH. A numerical analysis of the effects of nanofluid and porous media utilization on the performance of parabolic trough solar collectors. *Sustainable Energy Technologies and Assessments*. 2021 Jun 1; 45:101179.

[31] Biswal U, Chakraverty S, Ojha BK, Hussein AK. Numerical simulation of magnetohydrodynamics nanofluid flow in a semi-porous channel with a new approach in the least square method. *International Communications in Heat and Mass Transfer*. 2021 Feb 1;121: 105085.

[32] Hamid A, Khan M. Impacts of binary chemical reaction with activation energy on unsteady flow of magneto-Williamson nanofluid. *Journal of Molecular Liquids*. 2018 Jul 15; 262:435-42.

[33] Zeeshan A, Shehzad N, Ellahi R. Analysis of activation energy in Couette-Poiseuille flow of nanofluid in the presence of chemical reaction and convective boundary conditions. *Results in Physics*. 2018 Mar 1; 8:502-12.

[34] Gottmann P, Ouni M, Saussenthaler S, Roos J, Stirm L, Jähnert M, Kamitz A, Hallahan N, Jonas W, Fritsche A, Häring HU. A computational biology approach of a genome-wide screen connected miRNAs to obesity and type 2 diabetes. *Molecular Metabolism*. 2018 May 1; 11:145-59.

[35] Chu YM, Khan MI, Khan NB, Kadry S, Khan SU, Tlili I, Nayak MK. Significance of activation energy, bio-convection and magnetohydrodynamic in flow of third grade fluid (non-

Newtonian) towards stretched surface: A Buongiorno model analysis. *International Communications in Heat and Mass Transfer.* 2020 Nov 1; 118:104893.

[36] Khan AA, Bukhari SR, Marin M, Ellahi R. Effects of chemical reaction on third-grade MHD fluid flow under the influence of heat and mass transfer with variable reactive index. *Heat Transfer Research*. 2019; 50(11).

[37] Bhatti MM, Shahid A, Abbas T, Alamri SZ, Ellahi R. Study of activation energy on the movement of gyrotactic microorganism in a magnetized nanofluids past a porous plate. *Processes*. 2020 Mar;8(3):328.

[38] Muhammad T, Waqas H, Khan SA, Ellahi R, Sait SM. Significance of nonlinear thermal radiation in 3D Eyring–Powell nanofluid flow with Arrhenius activation energy. *Journal of Thermal Analysis and Calorimetry.* 2021 Jan;143(2):929-44.

[39] Mabood F, Khan W.A. and Ismail AI.Md, MHD boundary layer flow and heat transfer of nanofluids over a nonlinear stretching sheet: a numerical study. *Journal of Magnetism and Magnetic Materials*, 374 (2015), 569-576.

[40] Rama Bhargava and Harish Chandra Numerical simulation of MHD boundary layer flow and heat transfer over a nonlinear stretching sheet in the porous medium with viscous dissipation using hybrid approach. *Physics Fluid Dynamics*, (2017): arXiv:1711.03579

[41] Abdelsalam SI, Sohail M. Numerical approach of variable thermophysical features of dissipated viscous nanofluid comprising gyrotactic micro-organisms. *Pramana*. 2020 Dec;94(1):1-2.

[42] Sohail M, Naz R, Abdelsalam SI. Application of non-Fourier double diffusions theories to the boundary-layer flow of a yield stress exhibiting fluid model. *Physica A: Statistical Mechanics and its Applications*. 2020 Jan 1; 537: 122753.

[43] Kumar RK, Kumar GV, Raju CS, Shehzad SA, Varma SV. Analysis of Arrhenius activation energy in magnetohydrodynamic Carreau fluid flow through improved theory of heat diffusion and binary chemical reaction. *Journal of Physics Communications*. 2018 Mar 1;2(3):035004.

[44] Elsayed AF, Bég OA. New computational approaches for biophysical heat transfer in tissue under ultrasonic waves: The variational iteration and Chebyschev spectral simulations. *Journal of Mechanics in Medicine and Biology*. 2014 Jun 17;14(03):1450043.

[45] Bég OA, Hameed M, Bég TA. Chebyshev spectral collocation simulation of nonlinear boundary value problems in electrohydrodynamics. *International Journal for Computational Methods in Engineering Science and Mechanics*. 2013 Feb 1;14(2):104-15.

[46] Trefethen LN. *Spectral methods in MATLAB*. Society for Industrial and Applied Mathematics (SIAM); 2000 Jan 1.

[47] Rana P, Bhargava R. Flow and heat transfer of a nanofluid over a nonlinearly stretching sheet: a numerical study. *Communications in Nonlinear Science and Numerical Simulation*. 2012 Jan 1;17(1):212-26.

[48] Rashidi MM, Freidoonimehr N, Hosseini A, Bég OA, Hung TK. Homotopy simulation of nanofluid dynamics from a non-linearly stretching isothermal permeable sheet with transpiration. *Meccanica*. 2014 Feb; 49(2):469-82.

[49] Cortell R. Viscous flow and heat transfer over a nonlinearly stretching sheet. *Applied Mathematics and Computation*. 2007 Jan 15;184(2):864-73.

[50] Abdul Latiff NA, Uddin MJ, Bég OA, Ismail AI. Unsteady forced bioconvection slip flow of a micropolar nanofluid from a stretching/shrinking sheet. *Proceedings of the Institution of Mechanical Engineers, Part N: Journal of Nanomaterials, Nanoengineering and Nanosystems*. 2016 Dec; 230(4):177-87.

[51] J. Prakash, E.P. Siva, D Tripathi, S. Kuharat and O. Anwar Bég, Peristaltic pumping of magnetic nanofluids with thermal radiation and temperature-dependent viscosity effects: *modelling a solar magneto-biomimetic nanopump, Renewable Energy*, 133, 1308-1326 (2019).